

# Finite-temperature properties of non-magnetic transition metals: Comparison of the performance of constraint-based semi and nonlocal functionals

Leili Gharaee and Paul Erhart\*

*Chalmers University of Technology, Department of Physics, Gothenburg, Sweden*

Per Hyldgaard†

*Chalmers University of Technology, Department of Microtechnology and Nanoscience, MC2, Gothenburg, Sweden*

We assess the performance of nonempirical, truly nonlocal and semi-local functionals with regard to structural and thermal properties of  $3d$ ,  $4d$ , and  $5d$  non-magnetic transition metals. We focus on constraint-based functionals and consider the new consistent-exchange van der Waals density functional version vdW-DF-cx [Phys. Rev. B **89**, 035412 (2014)], the semi-local PBE [Phys. Rev. Lett. **77**, 3865 (1996)] and PBEsol functionals [Phys. Rev. Lett. **100**, 136406 (2008)] as well as the AM05 meta-functional [Phys. Rev. B **72**, 085108 (2005)]. Using the quasi-harmonic approximation structural parameters, elastic response, and thermal expansion at finite temperatures are computed and compared to experimental data. We also compute cohesive energies explicitly including zero-point vibrations. It is shown that overall vdW-DF-cx provides an accurate description of thermal properties and retains a level of transferability and accuracy that is comparable to or better than some of the best constraint-based semi-local functionals. Especially, with regard to the cohesive energies the consistent inclusion of spin polarization effects in the atoms turns out to be crucial and it is important to use the rigorous spin-vdW-DF-cx formulation [Phys. Rev. Lett. **115**, 136402 (2015)]. This demonstrates that vdW-DF-cx has general-purpose character and can be used to study systems that have both sparse and dense electron distributions.

## I. INTRODUCTION

The adiabatic connection formula (ACF) enables a formal determination of all exchange-correlation (XC) effects in density functional theory (DFT).<sup>1–3</sup> The XC energy density functional (DF)  $E_{xc}$  can be seen as the electrostatic binding of electrons with its associated XC hole. Good  $E_{xc}$  approximations represent the core of DFT and  $E_{xc}$  formulations reflect insight pertaining to the collective response of the interacting electron gas.<sup>2,3</sup> Important progress followed by enforcing hole conservation and other physical constraints in the formulation of the local density approximation (LDA) as well as semi-local functionals based on the generalized gradient approximation (GGA). Hole conservation underpins, for example, the PBE functional,<sup>4</sup> which has proven to be highly successful as a general-purpose functional for problems where the physical behavior is governed by the response at large electron concentrations. Specifically, the PBE functional is accurate for both hard materials and individual molecules and has accordingly found widespread applications.<sup>5</sup>

The last decade has witnessed the successful introduction of the van der Waals (vdW) density functional (vdW-DF) method,<sup>6–10</sup> launched as a systematic extension<sup>11–13</sup> of LDA and GGA. Unlike local and semi-local functionals such as the latter two it describes also the much larger class of sparse systems,<sup>14</sup> e.g., molecular solids, layered materials, and weak chemisorption cases, in which binding across internal voids arises from a truly nonlocal, vdW-type binding. The Chalmers-Rutgers vdW-DF method is focused on the electron response and has both regular releases (vdW-DF1,<sup>7</sup> vdW-DF2,<sup>15</sup> and vdW-DF-cx<sup>16</sup>) and variants (including vdW-DF-C09,<sup>17</sup> optB88, optPBE,<sup>18</sup> optB86b,<sup>19</sup> and rev-vdW-DF2<sup>20</sup>). It has recently been extended with a rigorous spin formulation that reflects the vdW-DF design logic.<sup>21</sup> There are also related but alternative formulations of the nonlocal-correlation

term in the Vydrov-van Voorhis family (VV09,<sup>22</sup> vdW-DF-09<sup>23</sup> and VV10<sup>24</sup>) and approaches that emphasize multipole response and mutual coupling of exchange holes.<sup>25–27</sup> In addition, there are approaches that focus on the dipole and multipole response of orbitals, atoms, and clusters (typically obtained outside of the ground-state DFT framework), compute the mutual coupling energy and add it to a traditional ground state DFT description.<sup>28–39</sup> It is commonly required that the chosen approach must be accurate both when there are important regions of low-electron concentration, i.e., sparse matter such as in intermolecular binding,<sup>14</sup> and when studying dense matter, i.e., harder materials such as transition metals.

The recent consistent-exchange version, vdW-DF-cx,<sup>9,13,16</sup> uses the vdW-DF plasmon-pole response description also to determine the *semilocal* component of the vdW-DF method. vdW-DF-cx is determined by a dielectric-response description that automatically enforces current conservation in the screening response.<sup>13,40</sup> The vdW-DF-cx method effectively uses the same plasmon-pole response to define both gradient-corrected exchange and nonlocal correlations. This new vdW-DF version thereby minimizes a hidden cross-over term  $\delta E_x^0$  that generally enters in the vdW-DF family of functionals.<sup>16</sup>

vdW-DF-cx has already proven itself accurate and useful in a number of problems that involve both regions of sparse and dense electron distributions such as molecular dimers,<sup>16,41</sup> layered materials,<sup>9,42–46</sup> semiconductors,<sup>9,47</sup> molecular crystals,<sup>48,49</sup> adsorption processes<sup>21,50</sup> as well as weak chemisorption, molecular switching, and molecular self assembly.<sup>21,50,51</sup> The ACF foundation and the emphasis on conservation laws in the vdW-DF-cx construction further suggests a general-purpose nature<sup>9</sup> and motivates a comprehensive investigation of its performance also for regular dense matter. This is particularly interesting since earlier members of the vdW-DF family have repeatedly been found to yield an inferior description of traditional bulk materials, in particular

the late transition metals.<sup>50</sup>

Here, we benchmark vdW-DF-cx for thermo-physical properties of non-magnetic transition metals, for which extensive experimental data is available for comparison.<sup>52,53</sup> Specifically, we consider lattice parameters, thermal expansion, and bulk moduli at finite temperature as well as the cohesive energies including zero-point contributions at the level of the quasi harmonic approximation (QHA). This data set explicitly tests not only the description of energy and structure but also forces, going beyond the set of properties commonly considered in comparative assessments of XC functionals. In addition to vdW-DF-cx we consider the constraint-based semi-local functionals, PBE,<sup>4</sup> PBEsol<sup>54</sup> and AM05.<sup>55</sup>

We show that vdW-DF-cx meets and exceeds the performance of the PBE, PBEsol and AM05 functionals for non-magnetic transition metals. This suggests that vdW-DF-cx provides a good, balanced description of nonlocal exchange and nonlocal correlation also in this type of materials. vdW-DF-cx thus remains a candidate for serving as a general-purpose materials-theory tool, working for both hard and soft matter.<sup>9</sup>

The remainder of this paper is organized as follows. The next section provides an overview of the constraint-based functionals considered in the present work while methodological aspects are compiled in Sect. III A. Section IV describes the main results before Sect. V provides a summary and conclusions. A detailed compilation of results including a per-element comparison with experimental data can be found in the Supplementary Material.<sup>56</sup>

## II. CONSTRAINT-BASED NONLOCAL FUNCTIONALS

### A. General aspects

Comparisons among constraint-based nonlocal functionals are valuable in our drive to further improve truly nonlocal DFs. Several previous studies have shown that some vdW-DF approaches can work well for solids.<sup>9,18–20,57</sup> While this has helped build trust in the vdW-DF method, constraint-based functionals such as vdW-DF-cx, PBE, PBEsol, and AM05 are all linked to the ACF and conservation<sup>4,13,16,55,58</sup> and can thus be expected to yield good transferability. Yet as briefly reviewed below different physical aspects were emphasized in their construction and one can thus expect to gain insight into strengths and limitations of each approach exactly because these functionals are each representatives of a specific design logic. By focusing the present benchmark on constraint-based functionals we are thus able to draw more general conclusions.

The four constraint-based functionals considered in the present work share some common traits while also having some distinct differences in their design logic, making it interesting to contrast their performance. All matter has internal surfaces with a variation between higher and lower electron density regions and insight from surface physics underpins all designs. It led Langreth and Perdew to the early GGA<sup>3</sup> and it entered the specification of gradient-corrected correla-

tion in PBEsol<sup>54</sup> and AM05.<sup>55</sup> These concepts are also central to the development of the vdW-DF method,<sup>6,10</sup> which takes the surface idea, however, further than in the GGA, noting that a semi-local representation of the electron-gas response does not retain a full description of the electro-dynamical coupling among (GGA) XC holes.<sup>6,10–13</sup> The electro-dynamical coupling is relevant, for example, when there are multiple interacting density fragments (molecules or surfaces) separated by a region with low electron concentration.<sup>13,59</sup>

The Fermi wave vector  $k_F(\mathbf{r}) = [3\pi^2 n(\mathbf{r})]^{1/3}$  sets a local energy scale via the LDA exchange energy per particle,  $\varepsilon_x^{\text{LDA}}(\mathbf{r}) = -(3/4\pi)k_F(\mathbf{r})$ . We take semi-local functionals to imply that the XC hole form or the energy per particle exclusively depend on the local (spin) density  $n(\mathbf{r})$  and the local scaled gradient  $s(\mathbf{r}) = |\nabla n|/[2n(\mathbf{r})k_F(\mathbf{r})]$ . Semi-local GGA functionals can be expressed via the local variation in the XC energy per particle

$$\varepsilon_{xc}^{\text{GGA}}(\mathbf{r}) \equiv F_{xc}(n(\mathbf{r}), s(\mathbf{r})) \varepsilon_x^{\text{LDA}}(\mathbf{r}). \quad (1)$$

Here, the XC enhancement factor  $F_{xc}(n(\mathbf{r}), s(\mathbf{r}))$  reflects the physical nature of the associated semi-local XC hole.<sup>4,54</sup>

### B. The PBE functional

The PBE functional<sup>4</sup> is an important example of a constraint-based GGA.<sup>5,60</sup> The PBE was designed by first constructing a numerical GGA with an enhancement factor  $\tilde{F}_{xc}$  that reflects conditions on the shape of the semi-local XC hole description and, in a subsequent step, by extracting an analytical form for the PBE  $F_{xc}$  for practical use. One can expect a high degree of transferability because it is anchored in conservation laws.<sup>2,3</sup> In fact the PBE functional has had a huge impact on materials theory and has turned out to be an extremely successful general-purpose functional for systems with dense electron distributions including both individual molecules and hard materials.<sup>5</sup>

### C. The PBEsol functional

One of the best performing constraint-based semi-local functionals for condensed matter is the PBEsol functional.<sup>54</sup> While, as in the case of PBE, the nature of screened many-body response and the XC hole were emphasized during its construction, its authors also relied on other formal results in its design. The GGA framework that underpins both PBE and PBEsol is very powerful but it is not possible to satisfy all constraints at the same time.<sup>61</sup> The PBE functional is highly transferable and works very well for both molecular formation energies and the structure and energies of hard materials. As a result of the diagrammatic (gradient-expansion) emphasis PBEsol yields an even better description of the structure of hard materials.<sup>54</sup>

### D. The AM05 functional

The AM05 constraint-based functional<sup>55</sup> performs very well for describing the structure of dense materials. It provides an, in principle, exact account of exchange effects for surfaces, i.e., the boundary between regions of higher and lower electron densities, whereas for internal regions this surface-exchange description is merged with that of the LDA. Like PBEsol, the AM05 functional extracts the gradient-corrected correlation from a study of the jellium surface energy. While it has different roots than PBE and PBEsol it is also constraint-based and can be viewed as a semi-local functional since it is possible to express the energy per particle variation using Eq. (1). Like the regular GGAs, it lacks an account of truly nonlocal correlation effects.

### E. The vdW-DF framework

The vdW-DF method<sup>6-8,10,12,16</sup> represents a systematic nonempirical extension of both LDA and the semi-local GGA description.<sup>9,13,21</sup> The very first version of this method was conceived two decades ago starting from a simple Ashcroft picture<sup>11</sup> of vdW binding in the itinerant electron gas.<sup>10,13</sup> It provides seamless integration with a GGA-type description while enforcing conservation laws on the underlying many-body response description.<sup>7,8,10,13</sup> The method predates the PBEsol and AM05 functionals and its origin<sup>12</sup> actually coincides with the launching of the PBE functional.<sup>4</sup> The vdW-DF method captures vdW forces among dimers in the asymptotic and the binding limits<sup>7,62-67</sup> as well as attraction between two-dimensional layers.<sup>42-44,59,68</sup> Importantly, it also captures the more general problem when nonlocal correlation forces compete with other types of forces,<sup>9</sup> for example, giving rise to binding across important regions of low electron densities.<sup>10,14</sup> The method was expected to be relevant in first-principle DFT for both pure vdW problems including regular physisorption,<sup>50,69-71</sup> porous-materials gas absorption,<sup>72-81</sup> and DNA base-pair interactions.<sup>82-86</sup> It was also quickly realized that truly nonlocal correlations affect materials descriptions much more broadly than what was perhaps originally anticipated.<sup>10,14,57,67,87-91</sup> The recent vdW-DF formulations are, for example, proving themselves valuable in the treatment of organic-inorganic interfaces and general weak-chemisorption problems.<sup>18,21,35,50,51,92-96</sup>

The vdW-DF framework formally constitutes an ACF recast<sup>7,10,13</sup>

$$E_{xc} = \int_0^\infty \frac{du}{2\pi} \text{Tr}\{\ln(\nabla\varepsilon(iu) \cdot \nabla G)\} - E_{\text{self}}. \quad (2)$$

Here,  $E_{\text{self}}$  and  $G$  denote the Coulomb self-energy and Green function, respectively,  $u$  is a complex frequency, and  $\varepsilon$  denotes a suitable approximation for a scalar, nonlocal dielectric function. The trace is over all spatial coordinates. The vdW-DF framework has exact screening and it defines  $\varepsilon$  via a plasmon-pole response description that reflects constraints like the  $F$  sum rule conservation.<sup>7,9,10,13</sup> The vdW-DF method

begins with a plasmon-pole approximation for screened response treated at the GGA level, i.e., by choosing  $\varepsilon(iu)$  so that it reflects the shape of an internal XC hole corresponding to a GGA-type semi-local functional  $E_{xc}^{\text{in}}$ . The vdW-DF method proceeds to define a semi-local and nonlocal functional components

$$E_{xc}^{\text{vdW-DF}} = E_{xc}^0 + E_c^{\text{nl}}, \quad (3)$$

where the semi-local component satisfies

$$E_{xc}^0 \approx E_{xc}^{\text{in}} \quad (4)$$

while the truly nonlocal XC energy term is defined as

$$E_c^{\text{nl}} = \int_0^\infty \frac{du}{2\pi} \text{Tr}\{\ln(\nabla\varepsilon(iu) \cdot \nabla G) - \ln(\varepsilon(iu))\}. \quad (5)$$

The vdW-DF framework can be interpreted as a rigorous implementation of the Ashcroft picture of vdW forces since Eq. (5) formally counts the shifts in electronic zero-point energies that arise with an electrodynamical coupling between the internal GGA-type XC holes.<sup>13</sup> In the most widely used general-geometry versions, the evaluation of Eq. (5) involves a second-order expansion that allows an efficient universal kernel formulation.<sup>7,8,10</sup> The vdW-DF versions are entirely nonempirical and rest solely on the physics that underpins the LDA XC energy and the GGA-type gradient-corrected exchange in  $E_{xc}^0$  and  $E_{xc}^{\text{in}}$ .

Here we benchmark the finite-temperature performance of the recent consistent-exchange version vdW-DF-cx.<sup>16</sup> In this functional the exchange component in  $E_{xc}^0$  is chosen to minimize

$$\delta E_x^0 \equiv E_{xc}^0 - E_{xc}^{\text{in}}, \quad (6)$$

for small-to-medium values of the scaled density gradient  $s$ . In practice, this means that  $\Delta E_x^0 = 0$  is for all systems but atoms and small molecules<sup>10,13,16</sup> so that vdW-DF-cx effectively serves as an implementation of (an expanded form of) the full vdW-DF framework Eq. (2).<sup>7,9,10,13</sup> Additional documentation for this new vdW-DF version can be found in Refs. 9, 10, and 13.

## III. METHODOLOGY

### A. Computational details

DFT calculations were carried out using the projector augmented wave (PAW) method<sup>97</sup> as implemented in the Vienna ab-initio simulation package (VASP).<sup>98</sup> For vdW-DF-cx calculations we used the patch released in Ref. 42. In primitive cell calculations the Brillouin zone was sampled using  $\Gamma$ -centered  $k$ -point grids with  $13 \times 13 \times 7$  divisions for hexagonal close packed (HCP) structures,  $14 \times 14 \times 14$  divisions for face-centered cubic (FCC), and  $15 \times 15 \times 15$  divisions for body-centered cubic (BCC) structures. The plane wave cutoff energy was chosen 30% larger than the commonly recommended value for each element in order to obtain very

well converged forces and especially stresses. The values employed are tabulated in Table V of the Supplementary Material, which also provides details concerning the PAW setups.

### B. Vibrational modeling

To evaluate finite temperature properties, we employed the quasi harmonic approximation (QHA). First, the harmonic Helmholtz free energy  $F(T, V)$  was evaluated as a function of temperature at fixed volume  $V$  according to<sup>99,100</sup>

$$F = \frac{1}{2} \sum_{q\nu} \hbar\omega_{q\nu} + k_B T \sum_{q\nu} \ln [1 - \exp(-\hbar\omega_{q\nu}/k_B T)]. \quad (7)$$

Here, the summations are the result of a discretization of the integral over the vibrational density of states and carried out over phonon modes with momentum  $\hbar\mathbf{q}$  and index  $\nu$ . The Gibbs free energy  $G(T, p)$  at constant pressure  $p$  is obtained by repeating the calculation of  $F(T, V)$  for a range of volumes and minimizing the sum of internal energy  $U(V)$ , Helmholtz energy  $F(T, V)$  and the pressure-volume term according to

$$G(T, p) = \min_V [U(V) + F(T, V) + pV]. \quad (8)$$

While the internal energy  $U(V)$ , here, simply corresponds to the Born-Oppenheimer energy as a function of volume, evaluation of the vibrational contribution Eq. (7) requires knowledge of the phonon dispersion on a dense  $\mathbf{q}$ -point mesh. To this end, force constants were calculated using the finite displacement method and  $4 \times 4 \times 4$  supercells. In the latter calculations the Brillouin zone was sampled using  $\Gamma$ -centered  $3 \times 3 \times 3$   $\mathbf{k}$ -point grids. The minimization in Eq. (8) was carried out over volumes ranging from  $0.85V_0$  to  $1.15V_0$ , where  $V_0$  is the volume corresponding to the minimum of the Born-Oppenheimer energy landscape.

Knowledge of the Gibbs free energy as a function of volume and temperature allows one to readily extract for example the lattice parameter(s), the bulk modulus and the thermal expansion coefficient(s) at finite temperatures. All of these quantities were analyzed using the PHONOPY package.<sup>100</sup>

Furthermore, we calculated the cohesive energy  $E_{\text{coh}}$  at zero Kelvin including the zero-point energy (ZPE) contribution,

$$E_{\text{coh}} = E_{\text{bulk}} + \frac{1}{2} \sum_{q\nu} \hbar\omega_{q\nu} - E_{\text{atom}}, \quad (9)$$

where  $E_{\text{bulk}}$  and  $E_{\text{atom}}$  denote the total energy of bulk material and atom, respectively. All terms in the latter equation were evaluated at the 0 K lattice constant corrected for zero-point effects.

### C. Atomic reference energies: spin effects

In general, spin-polarization must be included when calculating  $E_{\text{atom}}$ . While a consistent spin-polarized version of the

vdW-DF method was recently introduced<sup>21</sup> it has so far only been implemented in the QUANTUM-ESPRESSO package.<sup>101</sup> The vdW-DF evaluation of nonlocal correlations amounts to tracking the total energy shift that arises with the electro-dynamical coupling of plasmons, which, in turn, represent a GGA-type response to external fields.<sup>13</sup> The vdW-DF approximations that are implemented in VASP<sup>19</sup> are not fully consistent since they ignore the fact that spin polarization will itself adjust these plasmons.<sup>21</sup>

In the present study we therefore proceeded as follows in order to obtain atomic reference energies and eventually cohesive energies for vdW-DF-cx. We calculated the non-spin-polarized atomic energy  $E_{\text{atom}}^{\text{ns}, \text{vasp}}$  using VASP and then added the atomic spin polarization energy  $\Delta_{\text{spin}}^{\text{qe}}$  obtained using QUANTUM-ESPRESSO with the rigorous-spin vdW-DF-cx description.<sup>21</sup> That is we obtained the atomic energies as

$$E_{\text{atom}} = E_{\text{atom}}^{\text{ns}, \text{vasp}} + \underbrace{E_{\text{atom}}^{\text{sp}, \text{qe}} - E_{\text{atom}}^{\text{ns}, \text{qe}}}_{\Delta_{\text{spin}}^{\text{qe}}}. \quad (10)$$

In effect this procedure amounts to computing VASP and QHA-based cohesive-energy estimates  $E_{\text{coh}}^{\text{vasp}}$  and then adding a spin correction

$$\Delta_{\text{spin-corr}} = \Delta_{\text{spin}}^{\text{qe}} - \Delta_{\text{spin}}^{\text{vasp}}, \quad (11)$$

where  $\Delta_{\text{spin}}^{\text{vasp}} = E_{\text{atom}}^{\text{sp}, \text{vasp}} - E_{\text{atom}}^{\text{ns}, \text{qe}}$  represents the VASP approximation for the vdW-DF-cx atomic spin polarization energy. A detailed compilation of the atomic reference energies can be found in Table VI of the Supplementary Material.

In the QUANTUM ESPRESSO calculations of  $\Delta_{\text{spin}}$  we relied on norm-conserving pseudopotentials (NCPP) from the ABINIT package,<sup>102</sup> using a plane-wave (density) cutoff of 80 Ry (400 Ry) so as to best mimic the fact the VASP calculations are based on hard PAW setups. This NCPP choice was possible for all but the case of W, where the ABINIT NCPP did not yield the correct spin polarization state. For the W case alone we therefore relied on a W ultrasoft pseudopotential in calculating  $\Delta_{\text{spin-corr}}$ .<sup>103</sup>

## IV. RESULTS

### A. General assessment

In the following, we provide an overview of the key results from our comparative analysis of constraint-based XC functionals. A complete compilation of the data obtained with each XC functional including lattice constants can be found in the Supplementary Material. To measure and compare the performance of different functionals, we consider the mean absolute percentage error (MAPE) defined as

$$M = \frac{1}{N} \sum_k \left| \frac{A_{\text{DFT}}^{(k)} - A_{\text{expt}}^{(k)}}{A_{\text{expt}}^{(k)}} \right|, \quad (12)$$

where  $A_{\text{DFT}}^{(k)}$  and  $A_{\text{ref}}^{(k)}$  denote predicted and experimental values of a property of structure  $k$  and the average contains  $N$  samples.

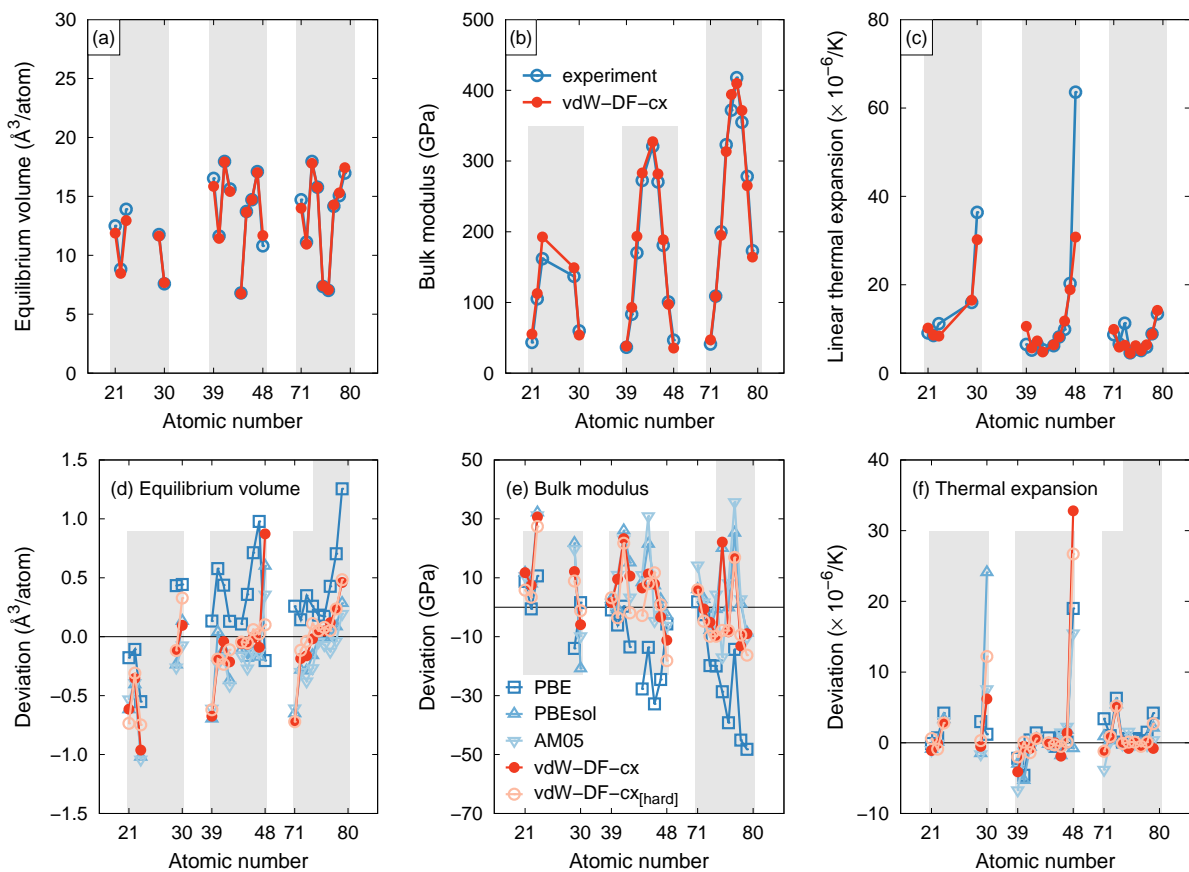


FIG. 1. Overview of thermophysical properties at 300 K obtained using the quasi-harmonic approximation in conjunction with density functional theory calculations. (a) Equilibrium volume, (b) bulk modulus, and (c) coefficient of average linear thermal expansion from experiment (Refs. 52 and 53) and calculations based on the vdW-DF-cx functional. Deviation between different XC functionals and experiment for (d) equilibrium volume, (e) bulk modulus, and (f) coefficient of linear thermal expansion. The shaded regions indicate the set of 3d, 4d, and 5d transition metals.

Many properties exhibit characteristic variations across the transition metal series, which follow the *d*-band filling [Fig. 1] and are reproduced by all XC functional considered here. While ZPE and thermal expansion effects are generally limited to a few percent of the volume, they are nonetheless crucial for an accurate assessment.

The performance comparison [Fig. 2 and Table I] confirms that PBEsol and, with the exception of the cohesive energy, also AM05 represent general improvements over PBE. The relatively large MAPEs [Table I] arise mostly from larger errors in just a few systems. In the case of PBE the MAPE for the cohesive energy of BCC structures is particularly large. This issue is primarily caused by an inaccurate description of the electronic configuration of the isolated spin-polarized atoms, which impacts the atomic reference energy.

More interestingly, the comparison demonstrates that the truly nonlocal vdW-DF-cx performs at least at the level of PBEsol and AM05. In fact, considering all properties vdW-DF-cx provides the best overall agreement with the experimental reference data. This is especially remarkable since previous non-empirical versions of the DF method, namely vdW-DF1<sup>7</sup> (in which exchange is approximated by the revPBE

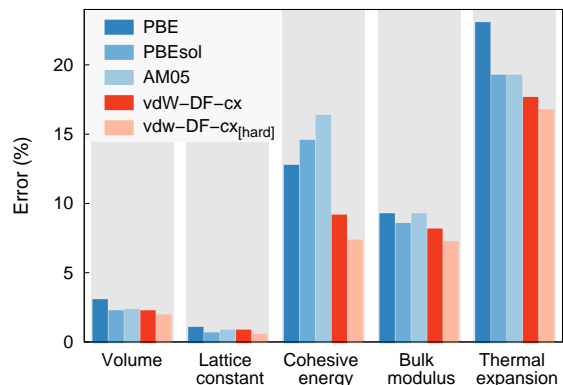


FIG. 2. Performance of different constraint-based XC functionals based on the data from Table I. The MAPEs were computed with regard to thermophysical properties measured at 300 K, with the exception of the cohesive energy, for which zero K values are compared.

functional<sup>104</sup>) and vdW-DF2<sup>15</sup> (in which exchange is approximated by a revised version<sup>105</sup> of the PW86 functional<sup>106</sup>) per-

TABLE I. Performance of constrained based XC functionals with respect to the description of thermophysical properties. The comparison includes the equilibrium volume  $V$ , bulk modulus  $B$ , as well as the linear coefficient of thermal expansion  $\alpha_l$  measured at room temperature, while in the case of the cohesive energy  $E_{coh}$  zero Kelvin data are compared, albeit including ZPE effects. Unless otherwise noted the calculations were carried out using standard PAW setups. The comparison comprises 11 HCP, 7 FCC, and 5 BCC elements.

Functional		$V$	$B$	$\alpha_l$	$E_{coh}$
vdW-DF-cx	HCP	3.0%	9.9%	20.6%	10.9%
	FCC	1.0%	5.0%	5.9%	9.5%
	BCC	1.9%	8.4%	27.3%	4.5%
	total	2.2%	8.1%	17.6%	9.1%
vdW-DF-cx (hard PAW setups)	HCP	2.6%	8.5%	17.7%	7.8%
	FCC	1.0%	4.9%	5.5%	8.7%
	BCC	1.7%	7.7%	30.0%	4.2%
	total	1.9%	7.2%	16.7%	7.3%
PBE	HCP	2.3%	7.1%	23.6%	10.9%
	FCC	4.6%	15.1%	11.8%	8.1%
	BCC	2.2%	5.6%	37.4%	23.3%
	total	3.0%	9.2%	23.0%	12.7%
PBEsol	HCP	2.8%	9.9%	21.7%	14.7%
	FCC	1.1%	6.1%	8.4%	12.4%
	BCC	2.6%	9.0%	28.7%	16.8%
	total	2.2%	8.5%	19.2%	14.5%
AM05	HCP	2.7%	11.3%	22.3%	25.7%
	FCC	1.2%	6.8%	6.8%	9.7%
	BCC	3.0%	7.8%	29.8%	4.8%
	total	2.3%	9.2%	19.2%	16.3%

form rather poorly for the late transition metals. In particular, in the case of Ag and Au the lattice constants are considerably overestimated in vdW-DF1 and vdW-DF2,<sup>19</sup> while vdW-DF-cx yields excellent results for these elements.

## B. Cohesive energies

Overall the constraint-based functionals considered here perform reasonably well with regard to the description of the cohesive energy [Fig. 3] although for most of the functionals there are problems with specific elements. Most notably, the vdW-DF-cx description clearly outperforms the other functionals in terms of the cohesive energies.

Moreover, the results demonstrate that the rigorous inclusion of spin effects in vdW-DF-cx<sup>21</sup> is important for an accurate description of the cohesive energy in nonmagnetic transition metals [Fig. 3(b)]. Since the atomic spin polarization energies are very large in the middle of the transition-metal bands [Fig. 3(c)], it is important to use the rigorous-spin vdW-DF-cx formulation.<sup>21</sup> The corrections are negative and systematically lead to larger values for  $\Delta_{spin}$  (see Table VI of the Supplementary Material). As a consequence our rigorous-spin vdW-DF-cx calculations provide a systematic improvement for the description of nonmagnetic transition metals, lowering for example the MAPE from 9.4% to 7.3% when using

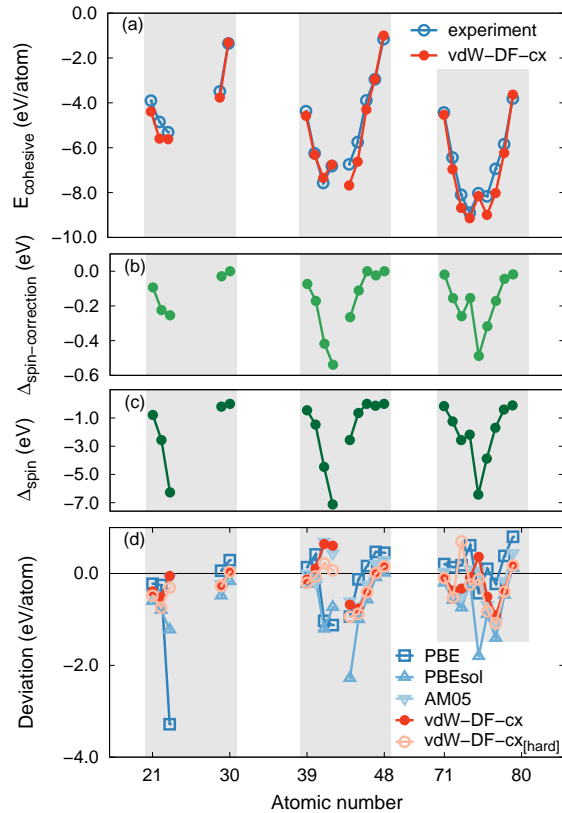


FIG. 3. (a) Cohesive energies at 0K obtained using the quasi-harmonic approximation in conjunction with density functional theory calculations from experiment (Ref. 52) and calculations based on the vdW-DF-cx functional including the spin correction according to Eq. (11). (b) Spin correction according to Eq. (11) that is added to the VASP-based description for our vdW-DF-cx benchmark to account for a rigorous description of spin effects in the atomic reference energies. (c) Atomic spin polarization energies  $\Delta_{spin}$  defined in Eq. (10) as calculated in the spin vdW-DF-cx formulation (available via QUANTUM-ESPRESSO calculations). (d) Deviation between different XC functionals and experiment for cohesive energies. The shaded regions indicate the set of 3d, 4d, and 5d transition metals.

hard PAW setups for vdW-DF-cx.

## C. Effect of PAW setups in the case of vdW-DF-cx

For computational efficiency it is often desirable to employ PAW setups that contain only the highest occupied states in the valence. This not only limits the total number of states in the calculation but also often allows using relatively large core radii that require smaller plane wave basis cutoffs in order to obtain converged results. While so far we have only considered results obtained using such “standard” PAW setups, it is now instructive to examine the choice of the PAW setup more closely. To this end, we exclusively consider calculations based on the vdW-DF-cx functional and “hard” PAW setups as detailed in Table V of the Supplementary Material.

Using the hard PAW setups systematically improves the

agreement with experiment, typically reducing the MAPE by a fraction of a percent (Table I and Fig. 2). Yet, the comparison clearly demonstrates that already the “standard” PAW setups yield very good result and are sufficient to achieve good results in many situations.

Cadmium represents an exception, for which there is pronounced difference between standard and hard setups. For example, the lattice constants at 300 K change from  $a = 3.168 \text{ \AA}$  and  $c = 5.373 \text{ \AA}$  to  $a = 3.023 \text{ \AA}$  and  $c = 5.512 \text{ \AA}$  when going from standard to hard PAW setups. The latter values are also in notably better agreement with the experimental numbers of  $a = 2.98 \text{ \AA}$  and  $c = 5.62 \text{ \AA}$  (Table II of the Supplementary Material). More generally, the late transition metals in HCP structure (Zn and Cd) are challenging for all XC functionals. This behavior is related to their special electronic structure that manifests itself e.g., in  $c/a$ -ratios (experimentally  $c/a = 1.89$  and  $1.86$  for Cd and Zn, respectively) that are considerably larger than in the ideal HCP structure ( $c/a = 1.633$ ).

#### D. Structure trends, semi-local and nonlocal functionals

The deviations between calculated and experimental data follow certain trends [Fig. 1(d-f)]. While PBE tends to overestimate the equilibrium volume, the other functionals are overall in rather close agreement with the reference data.

Contrasting specifically vdW-DF-cx and PBEsol performance (Fig. 4) shows that both functionals exhibit similar trends with respect to the variation of the accuracy with  $d$ -band filling. It is apparent that the data for the first and last columns of the series are slightly under and overestimated, respectively. The largest relative corrections of the volume arise for Zn and Cd and those elements also have some of the largest vibrational corrections to the cohesive energies. In fact, most DFs provide an inaccurate description of these elements, which as indicated above exhibit a HCP structure with a very large axial ratio.

Larger deviations from the reference data are also observed for V (BCC) for all functionals. We ascribed this behavior to the low temperature magnetism that has been reported in this element,<sup>107</sup> while in the present calculations it is treated without spin polarization.

Similar trends as for the equilibrium volume can be observed for bulk modulus [in reversed fashion, Fig. 1(e)] and linear coefficient of thermal expansion [Fig. 1(f)] although the errors are more scattered. The latter effect is probably connected to a larger uncertainty in the experimental data as will be discussed in the next section.

#### E. Bulk modulus and thermal expansion

So far we used experimental values from compilations of standard values<sup>52,53</sup> as reference data for equilibrium volumes (lattice constants), bulk moduli, and thermal expansion coefficients. While the data for lattice constants are usually very accurate, it must be acknowledged that measurements of bulk

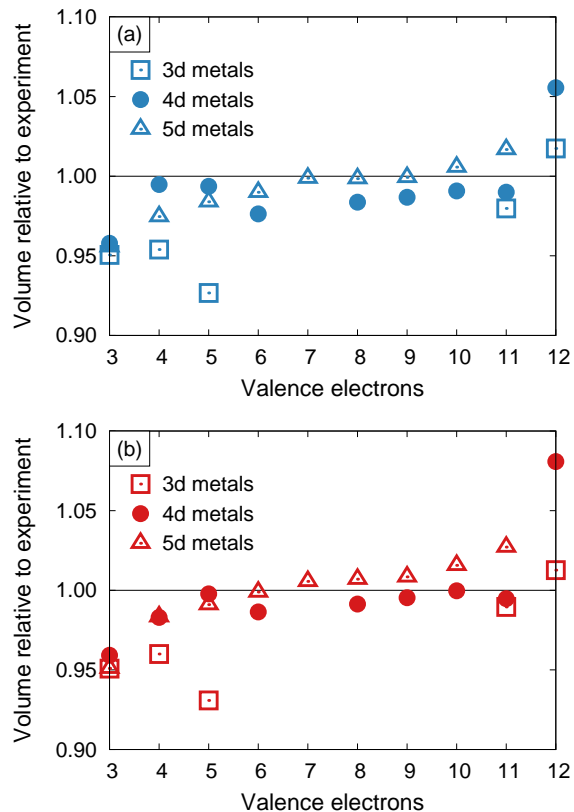


FIG. 4. Ratio of calculated to experimental equilibrium volumes for (a) PBEsol and (b) vdW-DF-cx (hard PAW setups). The transition from a volume underestimation converting to a volume overestimation is expected for GGAs and is found in both cases.

moduli and thermal expansion coefficients can carry rather significant errors, which are usually not documented in reference compendia. A closer inspection of experimental data available in the general scientific literature, however, reveals that at least in some cases these errors can be comparable or even exceed the deviation between the best performing XC functionals and experiment.

For illustration, we employ experimental data for the Young’s moduli  $E$  and Poisson ratios  $\nu$  of polycrystalline samples of the FCC metals Ir, Pt, and Rh.<sup>108</sup> As the experimental data range from 300 to 1500 K, this also allows us to compare experiment and calculations over a wide temperature span. The experimental data can be converted to bulk modulus using the relation  $B = E/3(1 - \nu)$ . This illustrates that there is considerable scatter in the experimental data with changing temperature that does not appear to be associated with a specific trend (Fig. 5); this is particularly pronounced in the case of Pt. The calculations overestimate the experimental data but overall the agreement is good with similar temperature dependence.

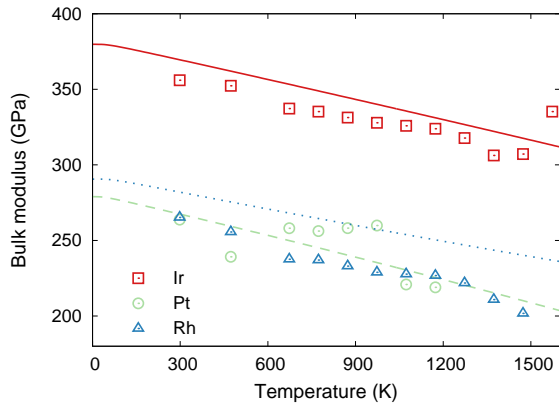


FIG. 5. Temperature dependence of bulk modulus from experiment and calculation (vdW-DF-cx). The experimental data points were obtained by converting the data for Young’s modulus  $E$  and Poisson ratio  $\nu$  measured in Ref. 108 using the relation  $B = E/3(1 - \nu)$ .

## F. General discussion

High accuracy and transferability of vdW-DF-cx had been previously indicated by a range of successful applications to systems that combine regions of both sparse and dense electron distributions.<sup>9,16,21,43,48–51</sup> In the present paper it has been demonstrated that, unlike the vdW-DF1 and vdW-DF2 versions, vdW-DF-cx also performs very well for hard materials.

The strong performance of PBEsol for traditional materials can be primarily traced to two of its features, namely a good form for gradient-corrected exchange and a good balance between this exchange part and the account of gradient-corrected correlation. The vdW-DF-cx strategy of seeking an ACF evaluation, see Eq. (2), implies picking a semi-local exchange component in  $E_{xc}^0$  that is given by diagrammatic expansion and therefore is similar to that of PBEsol in the low-to-medium  $s$  regime. Yet, vdW-DF-cx still replaces the PBEsol description of gradient-corrected correlation entirely with a truly nonlocal XC term  $E_c^{nl}$ . The fact that DF-cx performs at a PBEsol level with respect to hard materials thus suggests that vdW-DF-cx achieves a good balance between exchange and correlation. This observation makes it plausible that one can obtain further functional improvements by relying on the ACF recast, Eq. (2), for descriptions of nonlocal correlation effects.<sup>7,10,13,16</sup>

## V. SUMMARY

This study presents a comprehensive benchmark of constraint-based semi-local and non-local functionals with re-

spect to finite temperature thermophysical properties of non-magnetic transition metals. The main outcome of this comparison is that, unlike its predecessors in the vdW-DF family, the recently developed non-local vdW-DF-cx version achieves good transferability and accuracy also for hard materials. This is crucial, for example, for investigations of weakly-bound molecules at transition-metal surfaces. In the case of vdW-DF1 and vdW-DF2, the substantial overestimation of the lattice constants of the late transition metals, in particular Ag and Au, limited their application to these systems. The successful validation of vdW-DF-cx for these cases allows full ionic relaxation and thus tracking the impact of e.g., associated adsorption-induced surface modifications.<sup>9,19,51</sup>

In completing our work we found that Ambrosetti and Silvestrelli<sup>39</sup> recently presented a related benchmarking of how a range of functionals, including vdW-DF-cx, performs for the coinage metals. Our findings are consistent with their results but we have a broader scope as we consider the entire set of nonmagnetic transition metals and assess performance by comparing with experiments on a range of thermo-physical properties. This broader scope is instrumental for asserting the transferability of the method and provides a strong test of the robustness of the underlying physical input.

For the other functionals considered here the excellent performance is expected but it is interesting to note that the truly nonlocal functional vdW-DF-cx has as good if not better performance and transferability. This is encouraging for further development that builds of the vdW-DF framework.

Finally, we observe that quantitative comparisons as in the tables included in the Supplementary Material can also assist a crude benchmarking of future vdW-DF versions. This is because the tables implicitly provide a quantification of the net differences between the raw Kohn-Sham results and the associated room temperature characterizations that are relevant for comparison with most experimental observations.

## ACKNOWLEDGMENTS

We thank Kristian Berland for discussions. This work has been supported by the Swedish Research council (VR) and the Knut and Alice Wallenberg foundation as well as computer time allocations by the Swedish National Infrastructure for Computing at NSC (Linköping), HPC2N (Umeå), and C3SE (Gothenburg).

\* erhart@chalmers.se

† hyldgaard@chalmers.se

<sup>1</sup> J. Harris and R. O. Jones,

J. Phys. F: Metal Phys. **4**, 1170 (1974).

<sup>2</sup> O. Gunnarsson and B. I. Lundqvist, Phys. Rev. B **13**, 4274 (1976).

- <sup>3</sup> D. C. Langreth and J. P. Perdew, Phys. Rev. B **15**, 2884 (1977).
- <sup>4</sup> J. P. Perdew, K. Burke, and M. Ernzerhof, Phys. Rev. Lett. **77**, 3865 (1996).
- <sup>5</sup> K. Burke, J. Chem. Phys. **136**, 150901 (2012).
- <sup>6</sup> H. Rydberg, M. Dion, N. Jacobson, E. Schröder, P. Hyldgaard, S. I. Simak, D. C. Langreth, and B. I. Lundqvist, Phys. Rev. Lett. **91**, 126402 (2003).
- <sup>7</sup> M. Dion, H. Rydberg, E. Schröder, D. C. Langreth, and B. I. Lundqvist, Phys. Rev. Lett. **92**, 246401 (2004).
- <sup>8</sup> T. Thonhauser, V. R. Cooper, S. Li, A. Puzder, P. Hyldgaard, and D. C. Langreth, Phys. Rev. B **76**, 125112 (2007).
- <sup>9</sup> K. Berland, C. Arter, V. R. Cooper, K. Lee, B. I. Lundqvist, E. Schröder, T. Thonhauser, and P. Hyldgaard, J. Chem. Phys. **140**, 18A539 (2014).
- <sup>10</sup> K. Berland, V. R. Cooper, K. Lee, E. Schröder, T. Thonhauser, P. Hyldgaard, and B. I. Lundqvist, IOP Reports on Progress in Physics **78**, 066501 (2015).
- <sup>11</sup> K. Rapcewicz and N. W. Ashcroft, Phys. Rev. B **44**, 4032(R) (1991).
- <sup>12</sup> Y. Andersson, D. C. Langreth, and B. I. Lundqvist, Phys. Rev. Lett. **76**, 102 (1996).
- <sup>13</sup> P. Hyldgaard, K. Berland, and E. Schröder, Phys. Rev. B **90**, 075148 (2014).
- <sup>14</sup> D. C. Langreth, B. I. Lundqvist, S. D. Chakarova-Käck, V. R. Cooper, M. Dion, P. Hyldgaard, A. Kelkkanen, J. Kleis, L. Kong, S. Li, P. G. Moses, E. Murray, A. Puzder, H. Rydberg, E. Schröder, and T. Thonhauser, J. Phys. Condens. Matter **21**, 084203 (2009).
- <sup>15</sup> K. Lee, É. D. Murray, L. Kong, B. I. Lundqvist, and D. C. Langreth, Phys. Rev. B **82**, 081101 (2010).
- <sup>16</sup> K. Berland and P. Hyldgaard, Phys. Rev. B **89**, 035412 (2014).
- <sup>17</sup> V. R. Cooper, Phys. Rev. B **81**, 161104(R) (2010).
- <sup>18</sup> J. Klimeš, D. R. Bowler, and A. Michaelides, J. Phys. Cond. Matter **22**, 022201 (2010).
- <sup>19</sup> J. Klimeš, D. R. Bowler, and A. Michaelides, Phys. Rev. B **83**, 195131 (2011).
- <sup>20</sup> I. Hamada, Phys. Rev. B **89**, 123103 (2014).
- <sup>21</sup> T. Thonhauser, S. Zuluaga, C. A. Arter, K. Berland, E. Schröder, and P. Hyldgaard, Phys. Rev. Lett. **115**, 136402 (2015).
- <sup>22</sup> O. A. Vydrov and T. Van Voorhis, Phys. Rev. Lett. **103**, 063004 (2009).
- <sup>23</sup> O. A. Vydrov and T. Van Voorhis, J. Chem. Phys. **130**, 104105 (2009).
- <sup>24</sup> O. A. Vydrov and T. Van Voorhis, J. Chem. Phys. **133**, 244103 (2010).
- <sup>25</sup> A. D. Becke and E. R. Johnson, J. Chem. Phys. **127**, 154108 (2007).
- <sup>26</sup> A. D. Becke and E. R. Johnson, J. Chem. Phys. **123**, 154101 (2005).
- <sup>27</sup> A. D. Becke and E. R. Johnson, J. Chem. Phys. **122**, 154104 (2005).
- <sup>28</sup> S. Grimme, J. Comp. Chem. **27**, 1787 (2006).
- <sup>29</sup> A. Tkatchenko and M. Scheffler, Phys. Rev. Lett. **102**, 073005 (2009).
- <sup>30</sup> P. L. Silvestrelli, Phys. Rev. Lett. **100**, 053002 (2008).
- <sup>31</sup> P. L. Silvestrelli, J. Phys. Chem. A **113**, 5224 (2009).
- <sup>32</sup> S. Grimme, J. Antony, S. Ehrlich, and H. Krieg, J. Chem. Phys. **132**, 154104 (2010).
- <sup>33</sup> A. Ambrosetti and P. L. Silvestrelli, Phys. Rev. B **85**, 073101 (2012).
- <sup>34</sup> A. Tkatchenko, R. DiStasio, R. Car, and M. Scheffler, Physical Review Letters **108**, 236402 (2012).
- <sup>35</sup> V. G. Ruiz, W. Liu, E. Zojer, M. Scheffler, and A. Tkatchenko, Physical Review Letters **108**, 146103 (2012).
- <sup>36</sup> A. Ruzsinszky, J. P. Perdew, J. Tao, G. I. Csonka, and J. M. Pitarke, Phys. Rev. Lett. **109**, 233203 (2012).
- <sup>37</sup> J. Tao and J. P. Perdew, J. Chem. Phys. **141**, 141101 (2014).
- <sup>38</sup> J. Tao and A. M. Rappe, Phys. Rev. Lett. **112**, 106101 (2014).
- <sup>39</sup> A. Ambrosetti and P. L. Silvestrelli, Physical Review B **94**, 045124 (2016).
- <sup>40</sup> M. Dion, H. Rydberg, E. Schröder, D. C. Langreth, and B. I. Lundqvist, Phys. Rev. Lett. **92**, 246401 (2004).
- <sup>41</sup> P. Jurecka, J. Sponer, J. Cerny, and P. Hobza, Phys. Chem. Chem. Phys. **8**, 1985 (2006).
- <sup>42</sup> T. Björkman, J. Chem. Phys. **141**, 074708 (2014).
- <sup>43</sup> P. Erhart, P. Hyldgaard, and D. Lindroth, ACS Chemistry of Materials **27**, 5511 (2015).
- <sup>44</sup> D. O. Lindroth and P. Erhart, Phys. Rev. B **94**, 115205 (2016).
- <sup>45</sup> M. Muruganathan, J. Sun, T. Imamura, and H. Mizuta, Nano Letters **15**, 8176 (2015).
- <sup>46</sup> H. Sadeghi, S. Santarash, and L. C. J., Scientific Reports **5**, 9514 (2015).
- <sup>47</sup> M. Mehboudi, A. M. Dorio, W. Zhu, A. van der Zande, H. O. H. Churchill, A. A. Pacheco-Sanjuan, E. O. Harriss, P. Kumar, and S. Baraza-Lopez, Nano Letters **16**, 1704 (2016).
- <sup>48</sup> T. Rangel, K. Berland, S. Sharifzadeh, F. Brown-Altwater, K. Lee, P. Hyldgaard, L. Kronik, and J. B. Neaton, Phys. Rev. B **93**, 115206 (2016).
- <sup>49</sup> F. Brown-Altwater, T. Rangel, and J. B. Neaton, Phys. Rev. B **93**, 195206 (2016).
- <sup>50</sup> J. Löfgren, H. Grönbeck, K. Moth-Poulsen, and P. Erhart, J. Phys. Chem. C **120**, 12059 (2016).
- <sup>51</sup> B. Borca, V. Schendel, R. Petuya, I. Pentegov, T. Michnowicz, U. Kraft, H. Klauk, A. Arnau, P. Wahl, U. Schlickum, and K. Kern, ACS Nano **9**, 12506 (2015).
- <sup>52</sup> C. Kittel, *Introduction to Solid State Physics* (John Wiley & Sons, Inc., New York, Chichester, Brisbane, Toronto, Singapore, 1996).
- <sup>53</sup> [https://en.wikipedia.org/wiki/Thermal\\_expansion\\_coefficients\\_of\\_the\\_elements\\_\(data\\_page\)](https://en.wikipedia.org/wiki/Thermal_expansion_coefficients_of_the_elements_(data_page)).
- <sup>54</sup> J. P. Perdew, A. Ruzsinszky, G. I. Csonka, O. A. Vydrov, G. E. Scuseria, L. A. Constantin, X. Zhou, and K. Burke, Phys. Rev. Lett. **100**, 136406 (2008).
- <sup>55</sup> R. Armiento and A. E. Mattsson, Phys. Rev. B **72**, 085108 (2005).
- <sup>56</sup> See Supplementary Materials at XYZ for a detailed quantitative presentation of ab initio based modeling and for a per-element comparison with experimentally observed thermo-physical properties. Tables I, II, and III provide a detailed comparison at 300 K for structural and thermophysical properties of *3d*, *4d*, and *5d* nonmagnetic transition metals elements, respectively. Table IV represents a comparison of cohesive energies while Table V provides a specification of the PAW setups and the plane wave energy cutoffs used in the calculations of different elements. Finally, Table VI summarizes and compares the terms that enter the computation of the cohesive energy in the case of vdW-DF-cx.
- <sup>57</sup> E. Ziambaras, J. Kleis, E. Schröder, and P. Hyldgaard, Phys. Rev. B **76**, 155425 (2007).
- <sup>58</sup> J. P. Perdew, A. Ruzsinszky, G. I. Csonka, O. A. Vydrov, G. E. Scuseria, L. A. Constantin, X. Zhou, and K. Burke, Phys. Rev. Lett. **100**, 136406 (2008).
- <sup>59</sup> H. Rydberg, M. Dion, N. Jacobson, E. Schröder, P. Hyldgaard, S. I. Simak, D. C. Langreth, and B. I. Lundqvist, Phys. Rev. Lett. **91**, 126402 (2003).
- <sup>60</sup> A. D. Becke, J. Chem. Phys. **140**, 18A301 (2014).
- <sup>61</sup> The relation between PBE and PBEsol reflects in part the physical insight used for picking the form of gradient-corrected exchange enhancements.<sup>54</sup> Both functionals use conserving (albeit

- different) approximations for the semi-local XC hole. In the case of the PBE functional one arrives at a small- $s$  expansion that is also suggested by exact-scaling results for atomic-like high-density regions.<sup>5,54,60</sup> By contrast, in the construction of PBEsol one obtains a behavior consistent with diagrammatic results for pure exchange in the weakly perturbed electron gas.
- <sup>62</sup> A. Puzder, M. Dion, and D. C. Langreth, *J. Chem. Phys.* **124**, 164105 (2006).
- <sup>63</sup> S. Li, V. R. Cooper, T. Thonhauser, A. Puzder, and D. C. Langreth, *J. Phys. Chem. A* **112**, 9031 (2008).
- <sup>64</sup> K. Berland and P. Hyldgaard, *J. Chem. Phys.* **132**, 134705 (2010).
- <sup>65</sup> K. Berland, Ø. Borck, and P. Hyldgaard, *Comp. Phys. Comm.* **182**, 1800 (2011).
- <sup>66</sup> M. Callsen and I. Hamada, *Phys. Rev. B* **91**, 195103 (2015).
- <sup>67</sup> O. A. Vydrov, and T. Van Voorhis, in *Fundamentals of Time-Dependent Density Functional Theory*, edited by M. A. L. Marques, N. Maitra, F. Nogueira, E. K. U. Gross, and A. Rubio (Springer, Berlin, 2012).
- <sup>68</sup> D. C. Langreth, M. Dion, H. Rydberg, E. Schröder, P. Hyldgaard, and B. I. Lundqvist, *Int. J. Quan. Chem.* **101**, 599 (2005).
- <sup>69</sup> K. Lee, A. K. Kelkkanen, K. Berland, S. Andersson, D. C. Langreth, E. Schröder, B. I. Lundqvist, and P. P. Hyldgaard, *Phys. Rev. B* **84**, 193408 (2011).
- <sup>70</sup> K. Lee, K. Berland, M. Yoon, S. Andersson, E. Schröder, P. Hyldgaard, and B. I. Lundqvist, *J. Phys. Cond. Matter* **24**, 424213 (2012).
- <sup>71</sup> E. Londero, E. K. Karlson, M. Landahl, D. Ostrovskii, J. D. Rydberg, and E. Schröder, *J. Phys.: Condens. Matter* **24**, 424212 (2012).
- <sup>72</sup> Y. Yao, N. Nijem, J. Li, Y. J. Chabal, D. C. Langreth, and T. Thonhauser, *Phys. Rev. B* **85**, 064302 (2012).
- <sup>73</sup> K. Tan, N. Nijem, P. Canepa, Q. Gong, J. Li, T. Thonhauser, and Y. J. Chabal, *Chem. Mater.* **24**, 3153 (2012).
- <sup>74</sup> R. Poloni, B. Smit, and J. B. Neaton, *J. Phys. Chem. A* **116**, 4957 (2012).
- <sup>75</sup> H. Liu, V. R. Cooper, S. Dai, and D.-e. Jiang, *J. Phys. Chem. Lett.* **3**, 3343 (2012).
- <sup>76</sup> K. Lee, W. C. Isley, A. L. Dzubak, P. Verma, S. J. Stoneburner, L.-C. Lin, J. D. Howe, E. D. Bloch, D. A. Reed, M. R. Hudson, C. M. Brown, J. R. Long, J. B. Neaton, B. Smit, C. J. Cramer, D. G. Truhlar, and L. Gagliardi, *J. Am. Chem. Soc.* **136**, 698 (2014).
- <sup>77</sup> R. Poloni, K. Lee, R. F. Berger, B. Smit, and J. B. Neaton, *J. Phys. Chem. Lett.* **5**, 861 (2014).
- <sup>78</sup> K. Tan, S. Zuluaga, Q. Gao, N. Nijem, J. Li, T. Thonhauser, and Y. J. Chabal, *Chem. Mater.* **27**, 2203 (2015).
- <sup>79</sup> S. Zuluaga, E. M. A. Fuentes-Fernandez, K. Tan, F. Xu, J. Li, Y. J. Chabal, and T. Thonhauser, *J. Mater. Chem. A* **4**, 5176 (2016).
- <sup>80</sup> R. Poloni and J. Kim, *Int. J. Quant. Chem.* **116**, 569 (2016).
- <sup>81</sup> E. Kuisma, C. F. Hansson, T. B. Lindberg, C. A. Gillberg, S. Idh, and E. Schröder, *J. Chem. Phys.* **144**, 184704 (2016).
- <sup>82</sup> F. Ortman, W. G. Schmidt, and F. Bechstedt, *Phys. Rev. Lett.* **95**, 186101 (2005).
- <sup>83</sup> V. R. Cooper, T. Thonhauser, A. Puzder, E. Schröder, B. I. Lundqvist, and D. C. Langreth, *J. Amer. Chem. Soc.* **130**, 1304 (2007).
- <sup>84</sup> S. Li, V. R. Cooper, T. Thonhauser, B. I. Lundqvist, and D. C. Langreth, *J. Phys. Chem. B* **113**, 11166 (2009).
- <sup>85</sup> K. Berland, S. D. Chakarova-Käck, V. R. Cooper, D. C. Langreth, and E. Schröder, *J. Phys: Condens. Matter* **23**, 135001 (2011).
- <sup>86</sup> D. Le, A. Kara, E. Schröder, P. Hyldgaard, and T. S. Rahman, *J. Phys.: Condens. Matter* **24**, 424210 (2012).
- <sup>87</sup> S. D. Chakarova-Käck, O. Borck, E. Schröder, and B. I. Lundqvist, *Phys. Rev. B* **74**, 155402 (2006).
- <sup>88</sup> J. Kleis, E. Schröder, and P. Hyldgaard, *Phys. Rev. B* **77**, 205422 (2008).
- <sup>89</sup> K. Johnston, J. Kleis, B. I. Lundqvist, and R. Nieminen, *Phys. Rev. B* **77**, 121404 (2008).
- <sup>90</sup> K. Berland, T. L. Einstein, and P. Hyldgaard, *Phys. Rev. B* **80**, 155431 (2009).
- <sup>91</sup> J. Klimeš and A. Michaelides, *J. Chem. Phys.* **137**, 120901 (2012).
- <sup>92</sup> S. D. Chakarova-Käck, Ø. Borck, E. Schröder, and B. I. Lundqvist, *Phys. Rev. B* **74**, 155402 (2006).
- <sup>93</sup> S. D. Chakarova-Käck, E. Schröder, B. I. Lundqvist, and D. C. Langreth, *Phys. Rev. Lett.* **96**, 146107 (2006).
- <sup>94</sup> G. Li, I. Tamblyn, V. R. Cooper, H.-J. Gao, and J. B. Neaton, *Phys. Rev. B* **85**, 121409 (2012).
- <sup>95</sup> J. Maurer, V. G. Ruiz, and A. Tkatchenko, *J. Chem. Phys.* **143**, 102808 (2015).
- <sup>96</sup> A. Tkatchenko, L. Romaner, O. T. Hofmann, E. Zojer, C. Ambrosch-Draxl, and M. Scheffler, *MRS Bulletin* **35**, 435 (2010).
- <sup>97</sup> P. E. Blöchl, *Phys. Rev. B* **50**, 17953 (1994); G. Kresse and D. Joubert, *Phys. Rev. B* **59**, 1758 (1999).
- <sup>98</sup> G. Kresse and J. Hafner, *Phys. Rev. B* **47**, 558 (1993); G. Kresse and J. Furthmüller, *Phys. Rev. B* **54**, 11169 (1996).
- <sup>99</sup> D. C. Wallace, *Thermodynamics of Crystals* (Dover, Mineola, New York, 1998).
- <sup>100</sup> A. Togo and I. Tanaka, *Scr. Mater.* **108**, 1 (2015).
- <sup>101</sup> P. Giannozzi, S. Baroni, N. Bonini, M. Calandra, R. Car, C. Cavazzoni, D. Ceresoli, G. L. Chiarotti, M. Cococcioni, I. Dabo, A. D. Corso, S. de Gironcoli, S. Fabris, G. Fratesi, R. Gebauer, U. Gerstmann, C. Gougoussis, A. Kokalj, M. Lazzeri, L. Martin-Samos, N. Marzari, F. Mauri, R. Mazzarello, S. Paolini, A. Pasquarello, L. Paulatto, C. Sbraccia, S. Scandolo, G. Sclauzero, A. P. Seitsonen, A. Smogunov, P. Umari, and R. M. Wentzcovitch, *J. Phys.: Condens. Matter* **21**, 395502 (2009).
- <sup>102</sup> X. Gonze, G. M. Rignanese, M. Verstraete, J. M. Beuken, Y. Pouillon, R. Caracas, F. Jollet, M. Torrent, G. Zerah, M. Mikami, P. Ghosez, M. Veithen, J. Y. Raty, V. Olevanov, F. Bruneval, L. Reining, R. Godby, G. Onida, D. R. Hamann, and D. C. Allan, *Zeitschr. Kristall.* **220**, 558 (2005).
- <sup>103</sup> We also tested using the W NCPP while constraining the spin polarization to the correct configuration, which yields a vdW-DF-cx value for the cohesive energy of W that is in even better agreement with experiment than when using the ultrasoft pseudopotential.
- <sup>104</sup> Y. Zhang and W. Yang, *Phys. Rev. Lett.* **80**, 890 (1998).
- <sup>105</sup> E. D. Murray, K. Lee, and D. C. Langreth, *J. Chem. Theory Comput* **5**, 2754 (2009).
- <sup>106</sup> J. P. Perdew and Y. Wang, *Phys. Rev. B* **33**, 8800 (1986).
- <sup>107</sup> Y. M. Smirnov and V. A. Finkel, *Soviet Physics JETP* **22**, 750 (1966).
- <sup>108</sup> J. Merker, D. Lupton, M. Töpfer, and H. Knake, *Platinum Metals Review* **45**, 74 (2001).